RESEARCH ARTICLE

Special Section:

Simulations of Stratospheric Sulfate Aerosol Geoengineering with the Whole Atmosphere Community Climate Model (WACCM)

Key Points:
- SO$_2$ injections cause the tropical lower stratosphere to warm primarily in the tropics, regardless of injection latitude
- Interactive chemistry changes significantly the shortwave heating in the stratosphere due to SO$_2$ injections
- The period of the QBO lengthens due to equatorial SO$_2$ injections and shortens due to injections poleward of the equator

Supporting Information:
- Supporting Information S1

Correspondence to:
J. H. Richter,
jrichter@ucar.edu

Stratospheric Dynamical Response and Ozone Feedbacks in the Presence of SO$_2$ Injections

Jadwiga H. Richter[1] (ID), **Simone Tilmes**[1,2] (ID), **Michael J. Mills**[2] (ID), **Joseph J. Tribbia**[1] (ID), **Ben Kravitz**[3] (ID), **Douglas G. MacMartin**[4,5] (ID), **Francis Vitt**[2] (ID), and **Jean-Francois Lamarque**[1] (ID)

[1]Climate and Global Dynamics Laboratory, National Center for Atmospheric Research, Boulder, CO, USA, [2]Atmospheric Chemistry, Observations, and Modeling Laboratory, National Center for Atmospheric Research, Boulder, CO, USA, [3]Pacific Northwest National Laboratory, Richland, WA, USA, [4]Mechanical and Aerospace Engineering, Cornell University, Ithaca, NY, USA, [5]Department of Computing and Mathematical Sciences, California Institute of Technology, Pasadena, CA, USA

Abstract Injections of sulfur dioxide into the stratosphere are among several proposed methods of solar radiation management. Such injections could cool the Earth's climate. However, they would significantly alter the dynamics of the stratosphere. We explore here the stratospheric dynamical response to sulfur dioxide injections ∼5 km above the tropopause at multiple latitudes (equator, 15°S, 15°N, 30°S and 30°N) using a fully coupled Earth system model, Community Earth System Model, version 1, with the Whole Atmosphere Community Climate Model as its atmospheric component (CESM1(WACCM)). We find that in all simulations, the tropical lower stratosphere warms primarily between 30°S and 30°N, regardless of injection latitude. The quasi-biennial oscillation (QBO) of the tropical zonal wind is altered by the various sulfur dioxide injections. In a simulation with a 12 Tg yr^{-1} equatorial injection, and with fully interactive chemistry, the QBO period lengthens to ∼3.5 years but never completely disappears. However, in a simulation with specified (or noninteractive) chemical fields, including O$_3$ and prescribed aerosols taken from the interactive simulation, the oscillation is virtually lost. In addition, we find that geoengineering does not always lengthen the QBO. We further demonstrate that the QBO period changes from 24 to 12–17 months in simulations with sulfur dioxide injections placed poleward of the equator. Our study points to the importance of understanding and verifying of the complex interactions between aerosols, atmospheric dynamics, and atmospheric chemistry as well as understanding the effects of sulfur dioxide injections placed away from the Equator on the QBO.

1. Introduction

Solar Radiation Management (SRM) is a term used to describe a set of proposed geoengineering methods that aim to reduce incoming sunlight to cool the Earth, counteracting some of the effects of global warming (Crutzen, 2006). One of the most studied methods of conducting SRM is the use of stratospheric sulfate aerosols (English et al., 2012; Heckendorn et al., 2009; Niemeier et al., 2011; Niemeier & Timmreck, 2015; Pitari et al., 2014; Rasch, Crutzen, & Coleman, 2008; Tilmes et al., 2009). Proposals for this method often involve stratospheric injections of sulfur dioxide (SO$_2$). SO$_2$ oxidizes in the stratosphere to form sulfate aerosols. Stratospheric sulfate aerosols scatter a fraction of incoming sunlight back to space, leading to cooling of the Earth's surface. Similar cooling has been observed after major volcanic eruptions, such as the eruption of Mt Pinatubo in 1991, which injected large amounts of SO$_2$ into the stratosphere (e.g., Bluth et al., 1992). Thorough reviews of the fundamental science underpinning stratospheric SRM have been conducted by, for example, Rasch, Tilmes, et al. (2008) and the recent assessment by the U.S. National Academy of Science (NRC, 2015). The atmospheric effects of sulfate aerosols are not limited to surface climate and the radiative budget. Because the aerosols also absorb shortwave (SW) and longwave (LW) radiation (Ferraro et al., 2011), they heat the stratosphere, altering stratospheric dynamics (Stenchikov et al., 2002). Using a two-stream radiative transfer code, Ferraro et al. (2011) showed that a globally uniform sulfate aerosol layer (14.5 Tg total sulfate mass) between 17 and 22 km results in tropical heating of up to 6 K above the tropopause, and a slight cooling at the poles. Ferraro et al. (2011) attributed the tropical heating to flux convergence from absorption of LW radiative flux from the warm troposphere below and small LW radiative flux from the cold tropical lower stratosphere. Tilmes et al. (2009) used a fully interactive chemistry climate model to show that sulfate aerosols in the lower stratosphere result in heating of 1.5 K in the tropical lower stratosphere, with largest values in the tropics

(40°S to 40°N). In their study, they used a prescribed aerosol distribution similar to that seen after the Mt Pinatubo volcanic eruption. Using a global climate model with prescribed ozone chemistry and a fixed size aerosol distribution consistent with a very large tropical injection of stratospheric sulfate aerosols to counteract a 4xCO$_2$ forcing, Ferraro et al. (2015) found that SRM results in tropical lower stratosphere heating of up to 16 K. They also noted cooling in the NH polar stratosphere in DJF and attributed that change to a dynamical feedback associated with a strengthened Arctic polar vortex, as also found by Tilmes et al. (2009). Ferraro et al. (2015) also found the intensification of the NH polar vortex as a result of stratospheric aerosols and as a consequence a near elimination of Sudden Stratospheric Warmings (SSWs). Warming of the tropical lower stratosphere due to sulfate aerosols has several consequences for the climate system. It can lead to the strengthening of the polar vortex (Driscoll et al., 2012; Ferraro et al., 2015; Tilmes et al., 2009), modification of the quasi-biennial oscillation (Aquila et al., 2014), and can change the tropospheric tropical circulation (Ferraro et al., 2014). Additionally, changes in lower stratospheric temperatures can impact stratospheric chemistry, including concentrations of ozone (Tilmes et al., 2009). Recently, Jones et al. (2016) used a coupled atmosphere-ocean model with prescribed ozone concentrations to simulate SRM where sulfur dioxide was injected at the equator at an altitude between 23 and 28 km (14 Tg SO$_2$ yr^{-1} for the 2090–2100 time period). They showed that the lower stratosphere warms by ~2 K, and the period of the QBO increased from 27 to 31 months. All of the previous work on this topic, using Earth System Models of varying complexity, has shown heating in the tropical lower stratosphere and associated dynamical changes resulting from stratospheric sulfate aerosol geoengineering. However, detailed thermal budgets have not been analyzed. Such analyses can provide insight into the main drivers of heating resulting from sulfate aerosol geoengineering, revealing interactions between aerosol heating, dynamics, and chemistry. Moreover, previous thermodynamic budget analyses possibly have serious gaps, because they were carried out with models that did not interactively couple stratospheric dynamics, chemistry, and aerosol microphysical growth, which are the sources of key nonlinearities in the atmospheric response to stratospheric heating. Geoengineering with sulfate aerosols results in a significant net decrease in the ozone layer with maximum changes in middle and high latitudes, therefore delaying the projected recover of the ozone layer (e.g., Tilmes et al., 2009; Pitari et al., 2014) and significant impacts on surface UV (Tilmes et al., 2012). These changes are dependent on the projected concentrations of ozone destroying substances. Increasing stratospheric temperatures as a result of SO$_2$ injections speeds up ozone destroying cycles that are independent of heterogeneous chemistry on aerosol surfaces. Furthermore, increasing heterogenous reactions change ozone loss rates in different directions depending on altitude and latitude of injection. In addition, changes in water vapor in the stratosphere impact reaction rates. Changes in ozone can in turn affect the shortwave heating rates, and therefore temperature and dynamics of the atmosphere. Here we investigate in detail the temperature changes and dynamical responses of the stratosphere, to sulfur dioxide injections in CESM1(WACCM). In addition to considering changes in the radiative terms in the thermodynamic budget of the atmosphere, we also examine changes due to dynamics. Previous studies of sulfate geoengineering aerosols have primarily focused on changes in stratospheric heating due to changes in longwave and shortwave heating from aerosols; however, as will be demonstrated here, these changes only partly explain the dynamical changes sulfate aerosols induce in a complex Earth system. In this study, we focus on simulations in which all Earth system components, including chemistry, are fully coupled. In addition, we include a specified chemistry and aerosol simulation (described later) to isolate the role of dynamical changes without the interaction between aerosol changes and chemistry. This simulation demonstrates the large ozone feedbacks on the thermal budgets and on changes to the QBO. Lastly, previous studies have focused primarily on the dynamical response and QBO changes to tropical additions of SO$_2$ or aerosols. Robock et al. (2008) examined the climate response to Arctic as well as tropical injections. However, their work focused on examining surface rather than stratospheric responses. Here we investigate how the dynamical response of the stratosphere and QBO change when SO$_2$ is injected at different latitudes, both tropical and subtropical, described in detail by Tilmes et al. (2017). Section 2 summarizes the model and describes the simulations used in the study. Section 3 presents the results, and section 4 provides a summary of and conclusions from our findings.

2. Model Description and Simulations
2.1. Model Description
Here we use the Community Earth System Model, Version 1 with the Whole Atmosphere Community Climate Model as the atmospheric component (CESM1(WACCM)). CESM1 (WACCM) has fully coupled atmospheric, ocean, land, and sea ice components. The atmospheric model has a finite-volume dynamical core, horizontal

resolution of 0.95° latitude × 1.25° longitude, and 70 vertical layers with a model top near 140 km. It is based on the Community Atmosphere Model, version 5.0 (CAM5) (Neale et al., 2012) and includes nonorographic gravity wave parameterization following Richter et al. (2010) with modified tuning parameters for the higher horizontal resolution and QBO as described by Mills et al. (2016, 2017). CESM1 (WACCM) uses fully interactive stratospheric chemistry based on the Model for OZone And Related chemical Tracers, MOZART3 (Kinnison et al., 2007). CESM1(WACCM) includes a comprehensive radiative transfer scheme and a modal treatment of tropospheric aerosols following the three-mode version of the Modal Aerosol Model (MAM3) (Liu et al., 2012). MAM3 includes sulfate and is coupled to cloud microphysics as described by Mills et al. (2016). MAM3 handles prognostic aerosols in both the troposphere and the stratosphere. Mills et al. (2016) describe the extension of MAM3, which was originally restricted to tropospheric aerosols, to include stratospheric sulfate aerosols. MAM3 treats aerosols as internal mixtures of sulfate, mineral dust, sea salt, black carbon, and organic material (Liu et al., 2012). In the stratosphere, MAM3 aerosols are almost exclusively composed of sulfates, with the exception being small amounts of tropospheric aerosols that cross the tropopause. MAM3 handles sulfates resulting from stratospheric SO_2 injection and other sources (including carbonyl sulfide (OCS), dimethylsulphide (DMS), and tropospheric SO_2 pollution), as well as tropospheric aerosols. MAM3 aerosols are coupled to the chemistry, providing surfaces area densities for heterogeneous reactions that affect stratospheric ozone, as described in Mills et al. (2016). SO_2 in CESM1(WACCM) is not included in radiative calculations.

The land, ocean, and seaice components of CESM1(WACCM) are the Community Land Model version 4.0 (CLM4.0; Lawrence et al., 2011), the Parallel Ocean Program version 2 (POP2; Danabasoglu et al., 2012) and the Los Alamos sea-ice model (CICE 25 version 4; Holland et al., 2012). The land model was run with interactive carbon and nitrogen cycles, and the atmospheric and land components are coupled to the tropospheric chemistry components. Biogenic surface emissions are calculated online in CLM using the Model of Emissions of Gases and Aerosols from Nature (MEGAN), version 2.1 (Guenther et al., 2012). CESM1(WACCM) has an excellent representation of mean stratospheric dynamics and chemistry (Mills et al., 2017). This model also produces an internally generated QBO with an approximate period of 24 months. Because of the relatively coarse vertical resolution of this model (only 70 layers between surface and 140 km), the QBO is somewhat deficient in the lower stratosphere and the westerly phases only reach down to 60 hPa as compared to 100 hPa in observations. This is due to the inadequate representation of low-frequency Kelvin and Rossby gravity waves. The basic model climatology, chemistry, and response to volcanic aerosols were evaluated by Mills et al. (2017) in a historical simulation (1975–2015).

2.2. Simulations

The control simulation for this study is the extension of a validated present-day simulation, described by Mills et al. (2017), through the year 2100 with greenhouse gas concentrations following the Representative Concentration Pathway 8.5 (RCP8.5) scenario and ozone depleting substances, as described in Morgenstern et al. (2017). This is the same control simulation described by Tilmes et al. (2017), Kravitz et al. (2017), and MacMartin et al. (2017). We examine here in detail five geoengineering simulations with single-point SO_2 injections into the stratosphere at different latitudes and ~5 km above the tropopause. The latitudes and altitudes of the injections are as follows: Equator at 25 km, 15°S and 15°N at 25 km, 30°S and 30°N at 23 km. SO_2 injections are placed in the stratosphere continuously, in one model grid box (180°E/180°W) with a constant emission rate at each time step, between years 2040 and 2050, starting from atmospheric and ocean states of the control simulation in 2040. The annual injection amount of 12 Tg is distributed equally over the entire year. The simulations described here are the same as the high-altitude 12 Tg injections described by Tilmes et al. (2017).

In addition, in order to isolate the impact of interactive chemistry on stratospheric dynamics, we performed a simulation with the specified chemistry (SC) version of CESM1(WACCM) (Smith et al., 2014) for the equatorial (25 km) injection case. The physical parameterizations in the SC version of CESM1 (WACCM) are exactly the same as in the full interactive chemistry (IC) version. However, instead of running with interactive chemistry, the following constituents are prescribed from the control simulation: O_3, OH, NO_3, and HO_2. The aerosol distribution is prescribed from the IC simulation with the 12 Tg yr^{-1} equatorial injection. Comparing the SC simulation to the fully interactive simulation allows for quantification of the contribution of interactive chemistry to changes in stratospheric heating and dynamics. By prescribing the aerosol distribution from the IC version of the model, we are including the effects of interactive chemistry on the aerosol distribution, but those effects are second order.
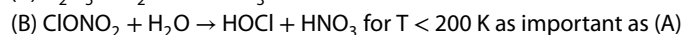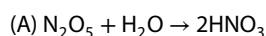
3. Results

3.1. Stratospheric Temperatures

We begin our analysis by examining the zonal mean temperature changes relative to the control simulation in the six simulations with stratospheric SO_2 injections (Figure 1). Figure 1a shows that as a result of the equatorial SO_2 injection, the lower stratosphere warms throughout the tropics, with maximum heating over 7 K near 60 hPa at the Equator. Enhanced longwave and shortwave heating, and therefore an increase in temperature, is expected to be associated with regions of increased sulfate aerosols (e.g., Ferraro et al., 2011). The majority of the stratospheric heating occurs in the regions of enhanced SO_4 mass, as depicted by the dashed contour. (Figure 6 of Tilmes et al., 2017, depicts and discusses in detail SO_4 mass changes in these simulations). However, the highest values of heating occur below, and not within the region of highest SO_4 mass (marked by the solid green line). In the simulation with 12 Tg yr^{-1} equatorial injection performed with the SC version of CESM1(WACCM), the temperature change is similar to that in the full interactive chemistry version. However, the temperature increase between 60 hPa and 100 hPa is 1 K smaller (Figure S1 in the supporting information), which is statistically significant, suggesting that interactive chemistry changes the nature of the temperature budget in this region, as we will demonstrate in detail in section 3.2. Figures 1c–1f show the zonal mean temperature changes resulting from SO_2 injections at 15°S, 15°N, 30°S and 30°N, respectively. Surprisingly, statistically significant increases in lower stratospheric heating remain throughout the tropics in both hemispheres, even though sulfate aerosols remain primarily in the hemisphere of injection. The maximum values of stratospheric heating are located near the maximum values of SO_4 mass. However, the heating extends well beyond the regions where the sulfate aerosols are concentrated. In the simulations with 30°S and 30°N injection, there is also very little change in stratospheric temperatures poleward of 50°N, despite the fact that there are substantial concentrations of SO_4 in the polar regions (Figures 1e and 1f). The maximum value of stratospheric heating decreases as the latitude of injection moves poleward. In the NH, especially in the simulations with injections at the equator, 15°N, and 30°N, there is also warming in the upper stratosphere poleward of 45°N, but it is not statistically significant according to a Student's t test (95% confidence interval).

3.2. Stratospheric Ozone

Although in this work we focus on the dynamical response to stratospheric SO_2 injections, changes in ozone significantly alter the atmospheric shortwave heating rates, and hence the dynamical response (as will be demonstrated below), and hence it is important to consider here. Stratospheric ozone is influenced by the temperature, dynamics, photochemical production, and various ozone destroying substances (here prescribed using future projections). An additional important factor that influences ozone chemistry is aerosols (Portmann et al., 1996; Solomon et al., 1996; Tilmes et al., 2008). The enhanced aerosol surface area density with increased sulfate burden impacts two heterogeneous reactions:

(A) $N_2O_5 + H_2O \rightarrow 2HNO_3$
(B) $ClONO_2 + H_2O \rightarrow HOCl + HNO_3$ for T < 200 K as important as (A)

Reaction A results in a decrease of the NO_x/NO_y equilibrium with increasing surface area density and therefore decreases the abundance of reactive nitrogen and therefore reduces the catalytic NO_x ozone loss cycles, while it increases the ClO_x, BrO_x and HO_x ozone loss cycles. This leads to a net decrease in ozone loss in the tropical midstratosphere, where the NO_x cycle is most important (Tilmes et al., 2009). Reaction B that is more important for colder temperatures, and therefore in polar regions, increases catalytic ClO_x and HO_x ozone loss cycles, leading to enhanced ozone depletion in those regions. Depending on the levels of total chlorine, which is expected to decrease in the future based on future projections following the phase out of ozone destroying substances, the net ozone loss can be accelerated with increasing aerosol burden. This has led to a substantial increase of ozone loss after volcanic eruptions, mostly pronounced at high latitudes (Tie & Brasscur, 1995). Furthermore, the increase in stratospheric water vapor that result from geoengineering increases the HO_x catalytic ozone loss cycles throughout the stratosphere. In our simulations we still see a substantial reduction in column ozone especially over the SH between 2040 and 2050.

In simulation with equatorial 12 Tg per year SO_2 injection there is a significant enhancement of SO_4 in the tropics as depicted by the green contour in Figure 1a. In this simulation, ozone increases in the midstratosphere (around 10 hPa in the tropics) and decreases around 30 hPa in the tropics and in the lower stratosphere in high latitudes (Figure 2a). The increase in ozone occurs right above the regions of highest SO_4 mass, whereas the decrease in ozone is coaligned with the region of largest SO_4 mass. In addition, water vapor has increased throughout the stratosphere by 1 ppb (not shown) due to the increase in tropopause temperatures.
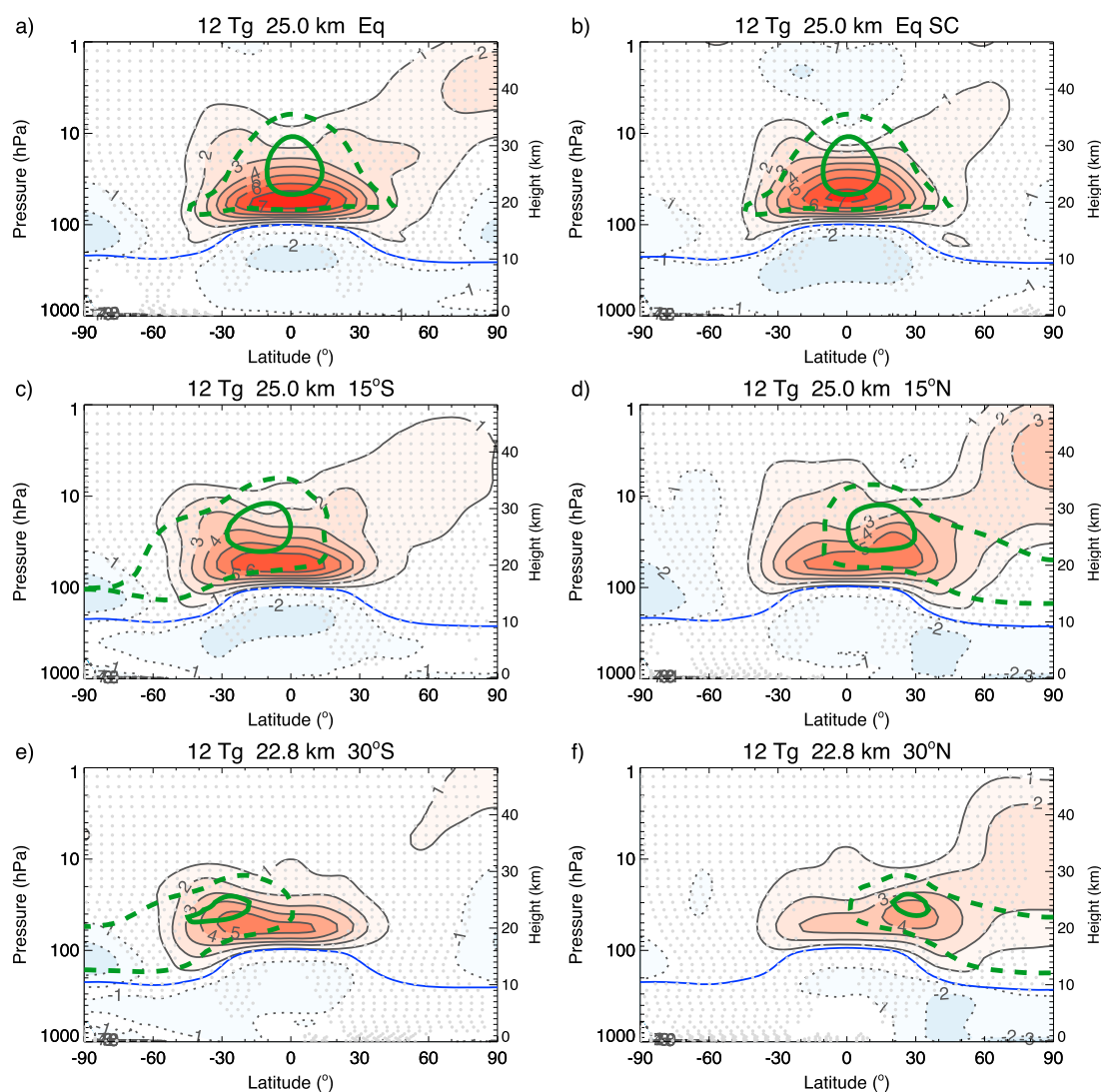
Figure 1. Temperature differences between various 12 Tg SO_2 yr^{-1} single injection simulations and control simulation, averaged between 2042 and 2049: (a) Equatorial 25 km, (b) Equatorial with specified chemistry 25 km, (c) 15°S 25 km, (d) 15°N 25 km, (e) 30°S 23 km, and (f) 30°N 23 km. Contour interval is 1.0 K. The zero contour is omitted. Areas not statistically significant at the 95% level based on a Student's t test are stippled. The green solid contour depicts an SO_4 mass mixing ratio of 40 μg S kg^{-1} air, and the dashed contour depicts a mixing ratio of 12 μg S kg^{-1} air.

Ozone loss cycles, dominated by the halogen loss in the lower stratosphere, result in the reduction of ozone, while the nitrogen cycle is more important in the middle stratosphere, resulting in an increase of ozone due to the reduction of NO_x. The HO_x cycle is important in the lower and upper stratosphere and likely contributes to the decrease of ozone in those regions.

In our simulations with injections poleward of the equator, ozone increases at some altitudes and decreases at others as shown in Figures 2c–2f for the 12 Tg 15° and 30° simulations. The maximum increase in the stratospheric ozone distribution occurs near 10 hPa and 20° in the same hemisphere as the SO_2 injection, as a result of the increase in aerosol burden and therefore heterogeneous reactions, as for the equatorial injections. In addition to changes in heterogeneous reactions, ozone is driven by changes in temperatures, water vapor, and transport. Increased temperatures and water vapor lead to increased photochemical ozone destruction from hydrogen and nitrogen cycles. This is demonstrated in Figure S2 showing the change of total odd oxygen chemical ozone loss rates. The changes in total odd oxygen chemical loss rates decrease where the NO_x cycle is reduced in the hemisphere of SO_2 injection and increased in the opposing hemisphere, as a result of the increase in temperature resulting in an increase in catalytic ozone destroying cycles. These changes contribute
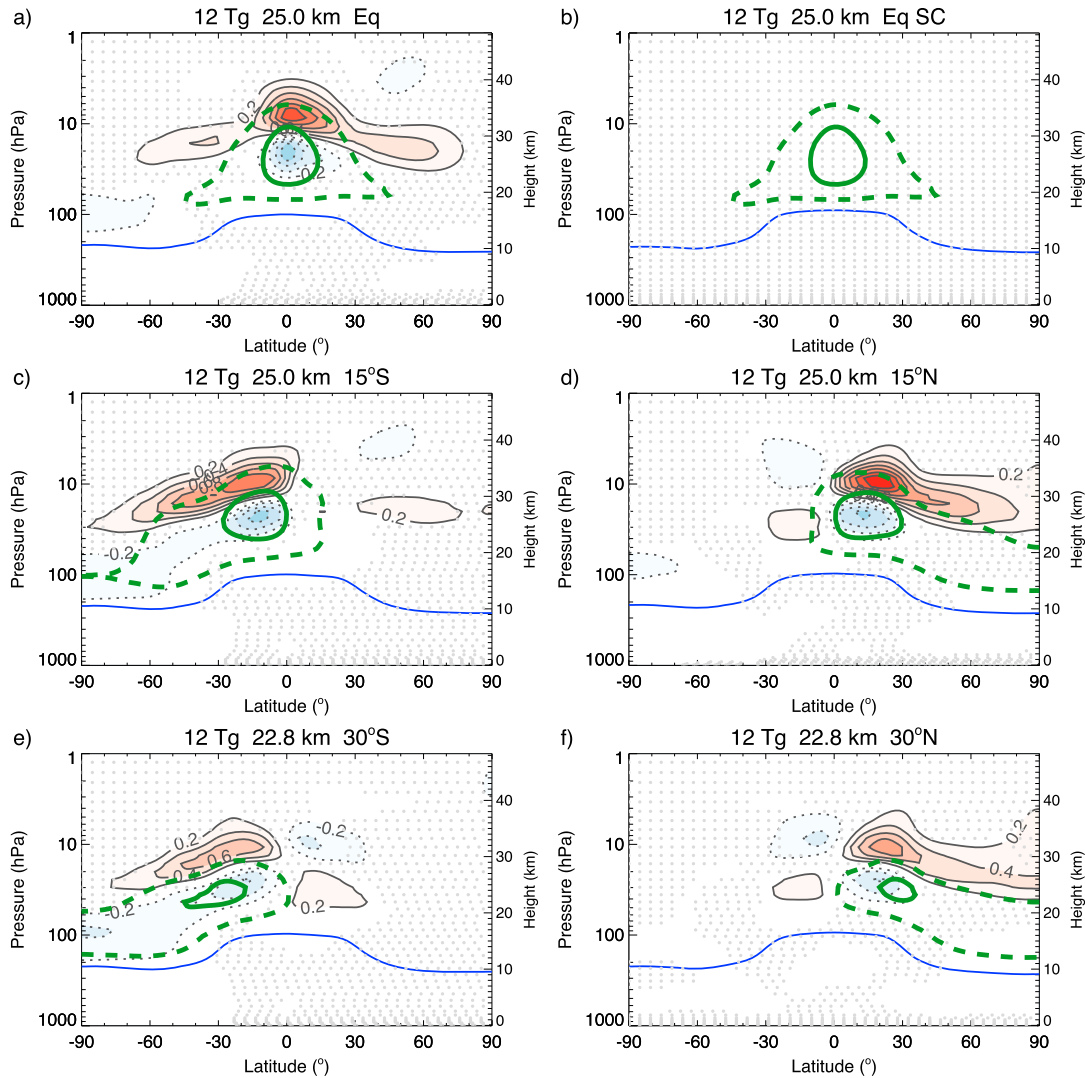
Figure 2. Same as Figure 1 but for ozone differences from control simulation. Contour interval is 0.2 ppm. The green solid contour depicts an SO_4 mass mixing ratio of 40 $\mu gS\ kg^{-1}$ air, and the dashed contour depicts a mixing ratio of 12 $\mu gS\ kg^{-1}$ air.

to opposite but smaller changes in ozone in the opposing hemisphere of the injection, where aerosols are not strongly enhanced.

3.3. Detailed Thermodynamic Budget

In this section we investigate in detail the thermodynamic budget of the stratosphere and explain many of the differences noted in the distribution of stratospheric heating for the six simulations we are examining. We consider the temperature budget using the Transformed Eulerian Mean (TEM) framework (Andrews et al., 1987). The TEM framework is preferred to an Eulerian framework for studies of the stratosphere and the Brewer Dobson Circulation as momentum and heat fluxes, which do not act separately, are included in one term. A review of the Brewer Dobson Circulation and TEM framework can be found in Butchart (2014). The zonal mean TEM temperature equation is

$$\bar{\theta}_t + a^{-1}\bar{v}^*\bar{\theta}_\phi + \bar{w}^*\bar{\theta}_z - \bar{Q} = -\rho_0^{-1}\left[\rho_0\left(\overline{v'\theta'}\,\bar{\theta}_\phi\,/\,a\bar{\theta}_z + \overline{w'\theta'}\right)\right]_z \tag{1}$$

where θ is the potential temperature, and $\bar{Q}$ is the total heating rate, a is the radius of the Earth, ϕ is the latitude, ρ_0 is the atmospheric density, and $\bar{v}^*$ and $\bar{w}^*$ are the mean residual vertical velocities defined as

$$\bar{v}^* \equiv \bar{v} - \rho_0^{-1}(\rho_0\,\overline{v'\theta'}\,/\,\bar{\theta}_z)_z \tag{2}$$

$$\bar{w}^* \equiv \bar{w} + (a\cos\phi)^{-1}(\cos\phi\,\overline{v'\theta'}\,/\,\bar{\theta}_z)_\phi \tag{3}$$
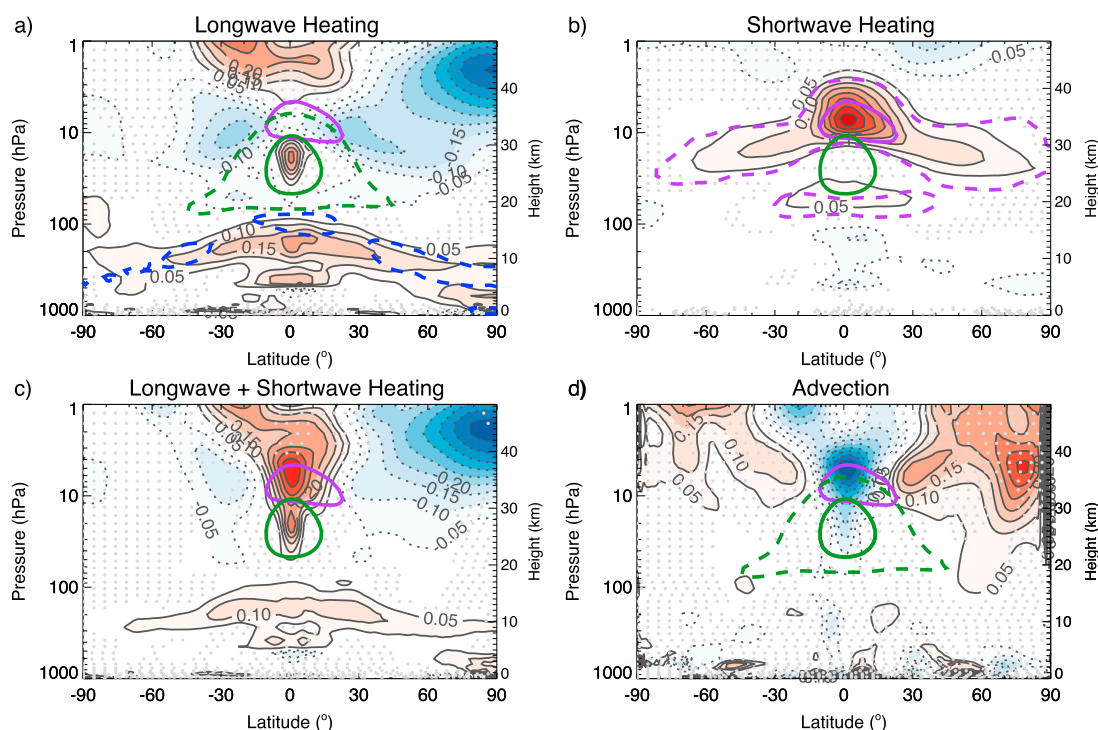
Figure 3. Annually averaged difference (between 2042 and 2049) of the following terms in the TEM zonal temperature equation (equation 1) for the 12 Tg SO$_2$ yr^{-1}, equatorial injection simulation and control: (a) longwave heating, (b) shortwave heating, (c) longwave and shortwave heating, and (d) advection. Contours are in equal intervals of 0.05 K d^{-1}. Areas not statistically significant at the 95% level based on a Student's *t* test are stippled. The solid and dashed green contours show differences of 0.05 and 0.15 μg kg^{-1} in SO$_4$ concentration between the two simulations. The dashed and solid purple contours depict the differences in ozone concentration of 0.05 and 0.6 ppm between the two simulations. Not all the green and purple contours are shown in all panels. The blue dashed contours show a change in total cloud fraction of −2.5%.

where *v* and *w* are the simulated meridional and vertical velocities. In (1)–(3), zonal mean quantities are marked with overbars, and departures from the zonal mean are denoted by primes. Subscripts ϕ and z denote latitudinal and height derivatives, respectively. Changes in temperature in the atmosphere result largely from the two main heating tendencies: advective and adiabatic heating/cooling ($a^{-1}\bar{v}^*\bar{\theta}_\phi + \bar{w}^*\bar{\theta}_z$) and radiative and diabatic heating/cooling ($\bar{Q}$). $\bar{Q}$ in CESM1(WACCM) consists of longwave and shortwave radiative heating, moist heating, dissipation heating from parameterized gravity waves, and diffusion (Andrews et al., 1987). The largest changes in the stratosphere between the simulation with and without SO$_2$ injections occur in the radiative heating rates. Moist heating changes are confined to the troposphere; they are not shown here, as the discussion focuses on explaining stratospheric heating changes. The largest contribution to the advective heating term comes from the vertical advection or adiabatic effect ($\bar{w}^*\bar{\theta}_z$); both terms are shown for completeness. The term on the right-hand side of (1) is the contribution to the heating from eddy forcing terms from nonquasigeostrophic motions. In the lower stratosphere, this term is much smaller than the other terms in the equation, so for the purposes of this discussion, we assume it to be negligible.

Figure 3 presents the changes in longwave and shortwave heating rates and advection calculated from the TEM temperature equation. Consistent with earlier studies (e.g., Ferraro et al., 2011, 2015), longwave heating (Figure 3a) has a local maximum in the region of highest SO$_4$ concentrations, near the equator at 20 hPa. Shortwave heating is also altered by SO$_2$ injection. However, the shortwave heating maxima correspond to the regions in which ozone concentration increases, and not in the regions where highest SO$_4$ concentrations occur (Figure 3b). This is an unexpected finding, and very different from previous findings using simpler models such as those by Ferraro et al. (2015) in which the largest changes in shortwave heating were associated with the highest concentrations of SO$_4$. The combination of longwave and shortwave radiative heating rate changes are shown in Figure 3c, and the adiabatic heating is shown in Figure 3d. In the stratosphere, the sum of longwave and shortwave heating balances diabatic heating in order to drive the atmosphere toward equilibrium. Hence, the longwave heating in the stratosphere acts to balance the changes to adiabatic heating/cooling.
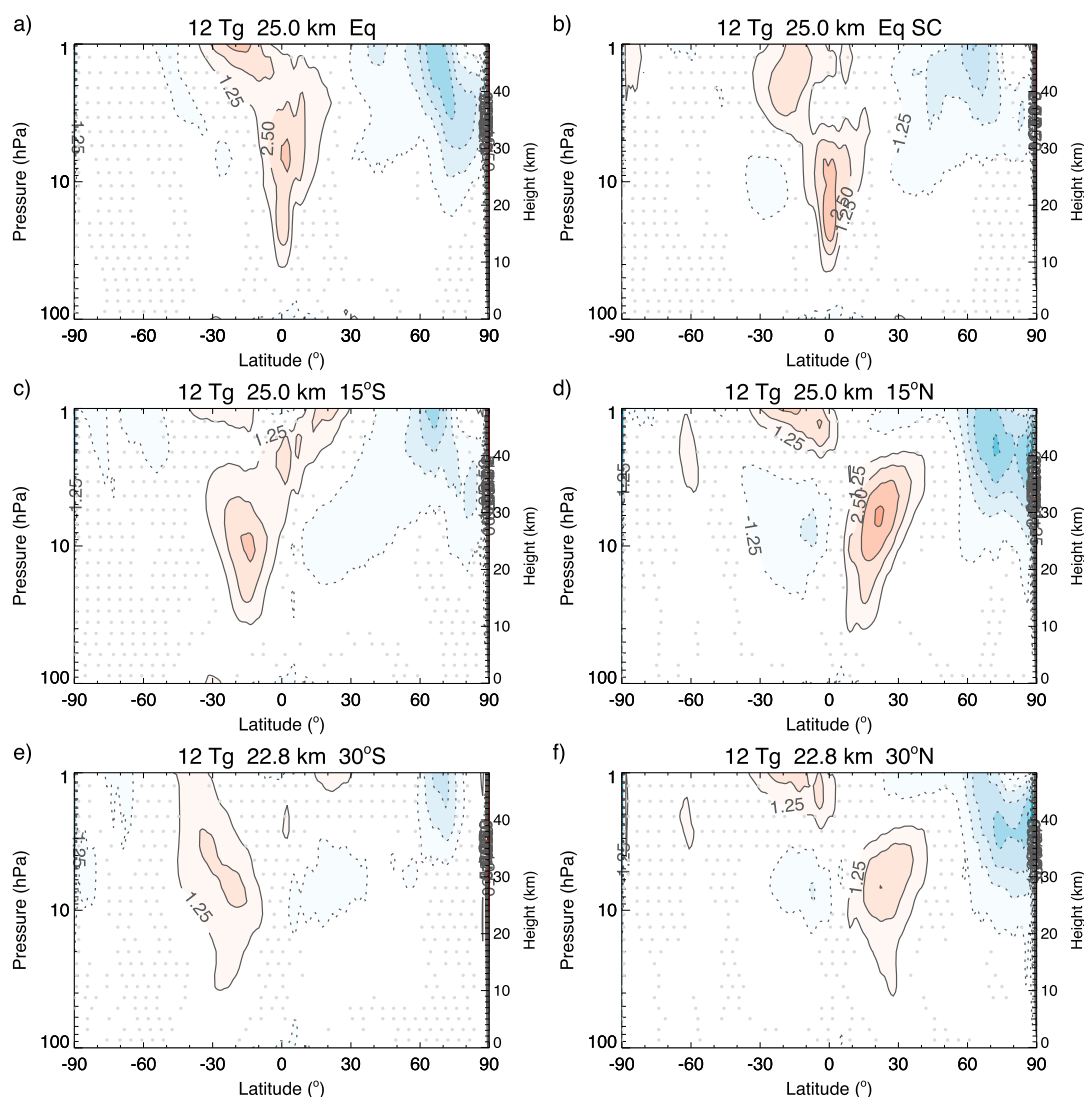
Figure 4. Residual vertical velocity differences from control for selected simulations with 12 Tg SO_2 yr^{-1} injections (averaged between 2042 and 2049) for (a) equatorial IC, (b) equatorial SC, (c) 15°S, (d) 15°N, (e) 30°S, and (f) 30°N simulations. Contour interval is 1.25×10^{-4} m s^{-1}. The zero contour is omitted. Areas not statistically significant at the 95% level based on a Student's t test are stippled.

Annually averaged TEM circulation consists of upwelling in the tropics and downwelling in the extratropics. Changes in the residual vertical velocity for all the simulations performed here are illustrated in Figure 4. Figure 4a shows that tropical SO_2 injection increases the mean upward residual vertical velocity in the tropics and decreases it primarily in the Northern Hemisphere, speeding up the Brewer Dobson Circulation (BDC) there. It is worthwhile to mention that differences in the strength of the Brewer Dobson circulation between the Northern and Southern Hemispheres, especially the deep branch, result in enhanced SO_4 concentration in the Northern Hemisphere. This is in detail explained in Tilmes et al. (2017). The adiabatic heating term in equation (1) is proportional to $-\bar{w}^*$ and hence is negative in the tropical stratosphere and positive outside of the 10°S to 10°N region. As such, warming in the stratospheric layer between 50°S and 50°N and 20 and 90 hPa is caused primarily by a combination of changes in shortwave and adiabatic heating. Longwave heating changes do occur in the region of highest aerosol concentrations. However, they primarily oppose the diabatic heating/cooling with a longwave heating increase in the equatorial stratosphere and longwave cooling in the subtropical stratosphere, especially in the Northern Hemisphere. Longwave heating also increases in the troposphere in the simulation with equatorial injection. This is due to the decrease in cloud fraction, especially for high clouds, as depicted by the blue dashed line in Figure 3a. Changes in adiabatic heating are accompanied by changes in convective heating (not shown as we focus on the stratospheric response
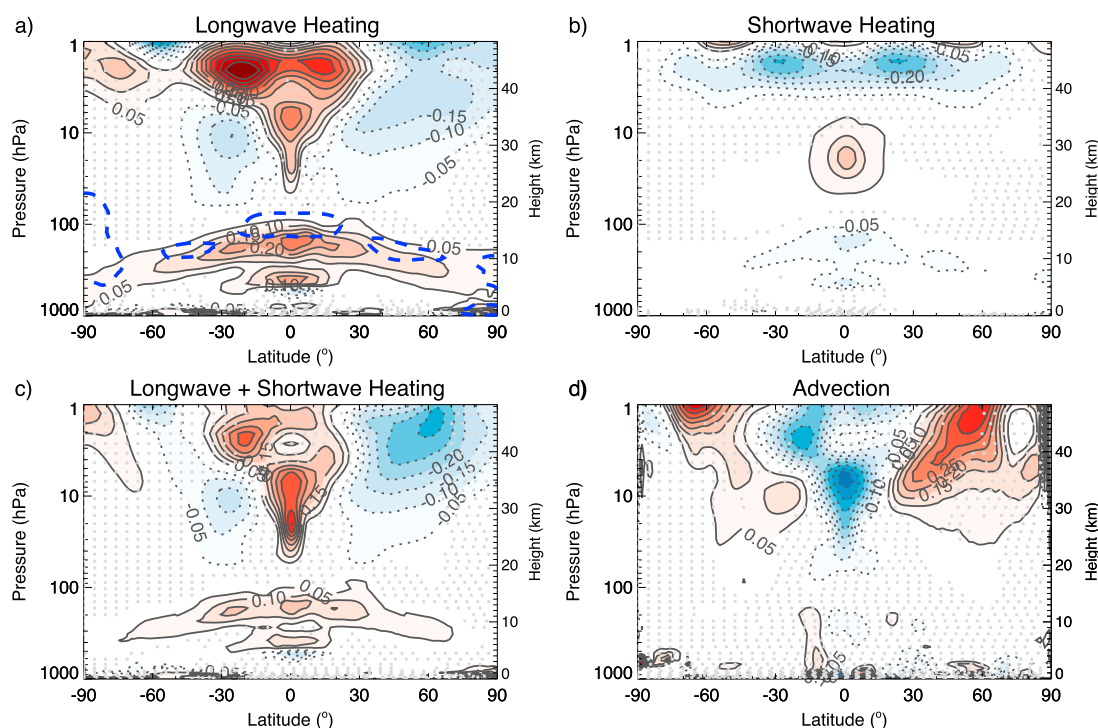
Figure 5. Same as Figure 3 but for the SC simulation with a 12 Tg SO_2 yr^{-1} equatorial injection.

here). Figure 3b shows that the largest change in shortwave heating is due to changes in ozone resulting from enhanced sulfate aerosols, as described above. There is almost a total absence of SW heating difference around 30 hPa in the simulation with equatorial SO_2 injection, where ozone is decreasing. However, many general circulation models do not use fully interactive chemistry when examining impacts of climate engineering using SO_2 injections. We now assess the impact of interactive chemistry on the changes in the thermal budget of the atmosphere by comparing heating terms shown in Figure 3 to those derived from the SC version of CESM1 (WACCM) (Figure 5). Figure 5a shows that when interactive chemistry is turned off, longwave heating changes due to an equatorial SO_2 injection are similar to those in the full chemistry simulation in the region of highest SO_4 mass. However, shortwave heating changes within the region of highest SO_4 concentrations are now positive, similar to the increase suggested by previous studies (e.g., Ferraro et al., 2011). This is because in the SC case, there is no ozone reduction in the aerosol layer to counteract the warming produced by the aerosols. There is also no change in shortwave heating above the aerosol layer as in the IC simulation. Thus, changes to ozone significantly alter the overall shortwave heating response to SO_2 injections by counteracting the changes in SW heating rates in the aerosol layer. Ozone is acting as a greenhouse gas and results in cooling from the reduction in ozone where aerosol concentrations are highest counteracting the warming from the absorption by the sulfate aerosols. The increase in ozone above the aerosol layer results in warming in that region.

The sum of LW and SW heating is similar between the SC and IC simulations; however, the differences in these cause slightly different changes to the BDC. The residual vertical velocity increases more between 10 and 40 hPa in the SC simulation (Figure 4b), causing differences in adiabatic warming/cooling (Figure 5d) as compared to the IC simulation. The longwave heating then responds to these changes. Because of the general similarities in changes in total radiative and adiabatic heating terms, the temperature differences resulting from SO_2 injection in the SC and IC simulations are very similar, however slightly larger in the SC as compared to the IC simulation (Figures 1a and 1b). Figure 1 illustrates that lower stratospheric heating due to SO_2 injections at latitudes poleward of the equator is mainly concentrated in the Tropics, despite the fact that the SO_4 mass spreads all the way to the poles. To understand this, we look at the detailed heat budget changes associated with SO_2 injection at 30°N (Figure 6). Figure 6a shows that longwave heating increases only near the region of highest SO_4 mass concentrations (and not within the entire aerosol layer), and there is very little change in shortwave heating in the entire aerosol layer. Instead, similarly to the simulation with
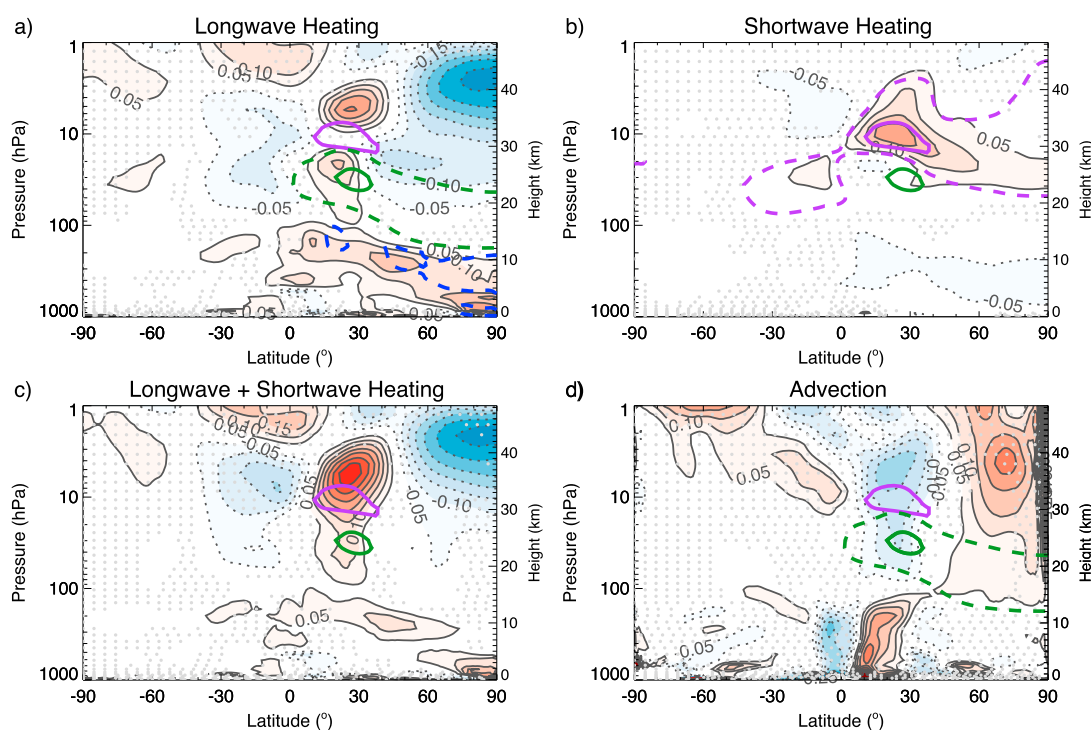
Figure 6. Same as Figure 3 but for the simulation with a 12 Tg SO_2 yr^{-1} 30°N injection.

equatorial injection, shortwave heating increases in regions of increased ozone concentration (Figure 6b). Shortwave heating increases primarily in the vicinity of 30°N and 10 hPa (Figure 6b) and adiabatic heating increases largely south of the equator and north of ~40°N, causing temperature increases of ~2 K away from regions of highest SO_4 concentration. As in the simulation with equatorial SO_2 injection, longwave heating attempts to balance the diabatic heating, with largest positive heating rates in region of adiabatic cooling, and largest decrease in regions of diabatic warming. Changes in the detailed heat budget for the 30°S, 15°N, and 15°S injection simulations are analogous to those of the simulation with a 30°N SO_2 injection (not shown): increased longwave heating occurs in the vicinity of highest SO_4 mass, and the largest changes in shortwave heating occur above that region, where the largest changes in ozone occur. The largest increases in the residual vertical velocity occur in regions of largest increase in total radiative heating, as shown in Figures 4c–4e, speeding up the annually averaged BDC.

3.4. Zonal Mean Wind and the Quasi-Biennial Oscillation

Changes in the zonal mean temperature and the BDC in the simulations with SO_2 injections are also associated with changes in the zonal mean wind patterns throughout the atmosphere. The zonal mean winds are in approximate thermal wind balance, meaning that increased latitudinal temperature gradient will be associated with increased vertical wind shear. In the equatorial stratosphere, the zonal mean wind is driven by a balance between vertical advection, gravity wave drag from small scale waves, and momentum deposition from larger scale waves such as Kelvin and mixed Rossby gravity waves. The balance between those terms determines the period and the amplitude of the QBO.

The annual, zonal mean wind changes for the six simulations examined here are shown in Figure 7. In simulations with an equatorial SO_2 injection, there is a statistically significant increase in tropical winds between 10 and 40 hPa of up to 6 m s^{-1} in the simulation with interactive chemistry and up to 8 m s^{-1} in the simulation with SC. In simulations with SO_2 injections away from the equator, it is also the tropical stratospheric winds that are primarily impacted. However, in the simulations with 15°S and 30°S injections, the winds slow down south of the equator and speed up north of the equator, between 10 and 30 hPa. In the simulations with 15°N and 30°N injections, the tropical winds slow down between the equator and 20°N, between 10 and 30 hPa. In all of the simulations shown in Figure 7, there is a statistically significant (per a Student's *t* test) decrease of 2 to 4 m s^{-1} of the upper tropospheric winds near 30°S and 100 hPa. In all of the simulations with SO_2 injections, there are also changes in the extratropical stratosphere, but those changes are not statistically significant,
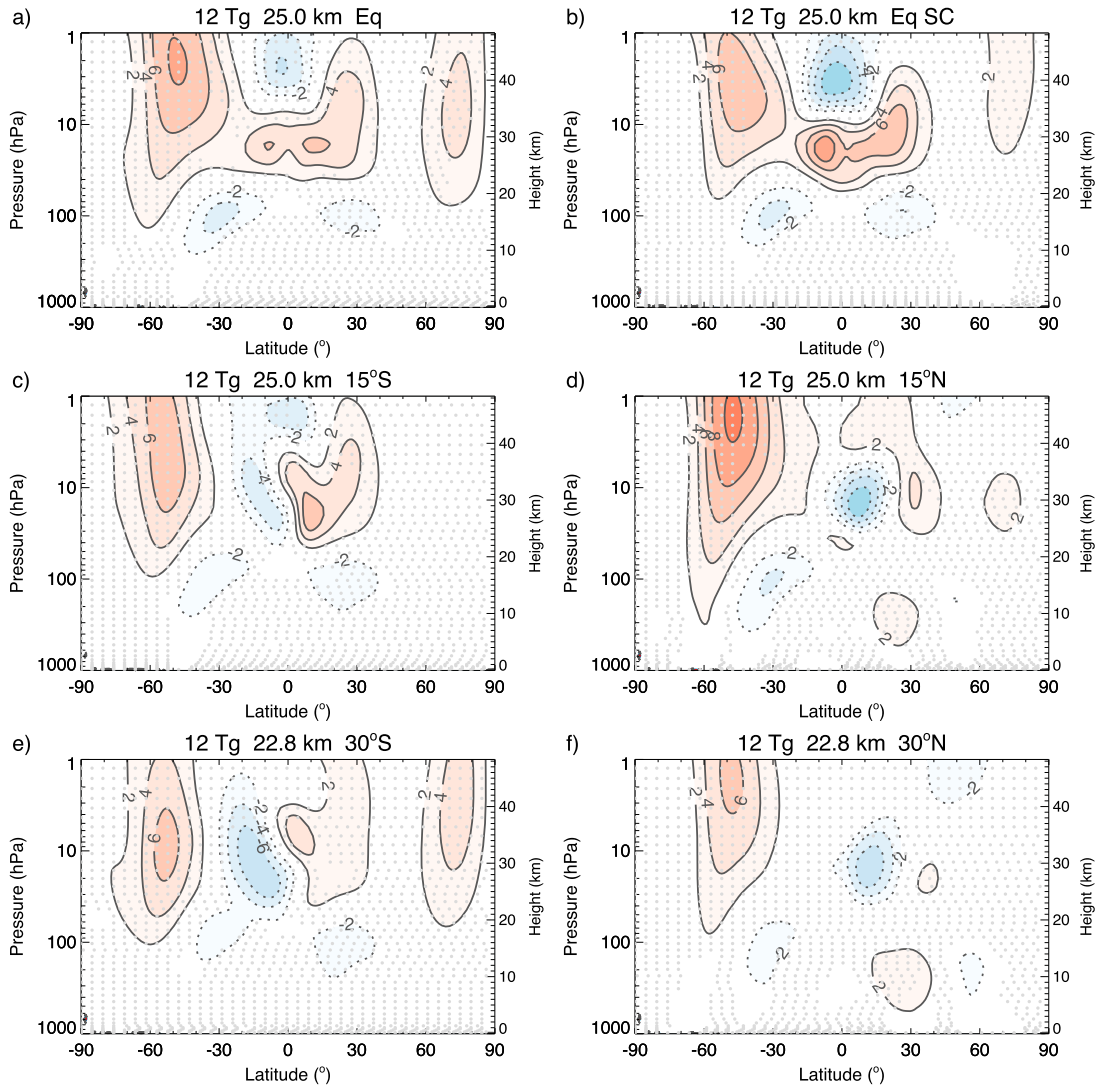
Figure 7. Same as in Figure 1 but for zonal mean wind. Contour interval is 2 m s^{-1}.

likely due to the short (10 year) length of the simulations. The changes in the tropical zonal mean wind due to SO$_2$ injections are best illustrated by looking at the QBO and considering the QBO forcing terms in these simulations. The changes in zonal mean wind with time are described by the TEM zonal wind equation:

$$\bar{u}_t = -\bar{v}^* \left[(a \cos\phi)^{-1} (\bar{u} \cos\phi)_\phi - f \right] - \bar{w}^* \bar{u}_z + \bar{X} + (\rho_0 \, a \cos\phi)^{-1} \nabla \cdot \mathbf{F} \qquad (4)$$

where the first term on the right-hand side is the meridional advection and Coriolis torque (f is the Coriolis parameter), the second term is vertical advection, $\bar{X}$ is the gravity wave drag, and the last term on the right-hand side of (4) is the Eliassen-Palm flux divergence from resolved waves (Andrews et al., 1987). The meridional and vertical components of the EP flux vector, $\mathbf{F}$, are defined as follows:

$$F^{(\phi)} \equiv \rho_0 \, a \cos\phi \, (\bar{u}_z \, \overline{v'\theta'} \, / \, \bar{\theta}_z - \overline{v'u'}) \qquad (5)$$

$$F^{(z)} \equiv \rho_0 \, a \cos\phi \left\{ \left[f - (a \cos\phi)^{-1} (\bar{u} \cos\phi)_\phi \right] \overline{v'\theta'} \, / \, \theta_z - \overline{w'u'} \right\} \qquad (6)$$

EP flux divergence is defined as

$$\nabla \cdot \mathbf{F} \equiv (a \cos\phi)^{-1} \frac{\partial}{\partial \phi} (F^{(\phi)} \cos\phi) + \frac{\partial F^{(z)}}{\partial z} \qquad (7)$$
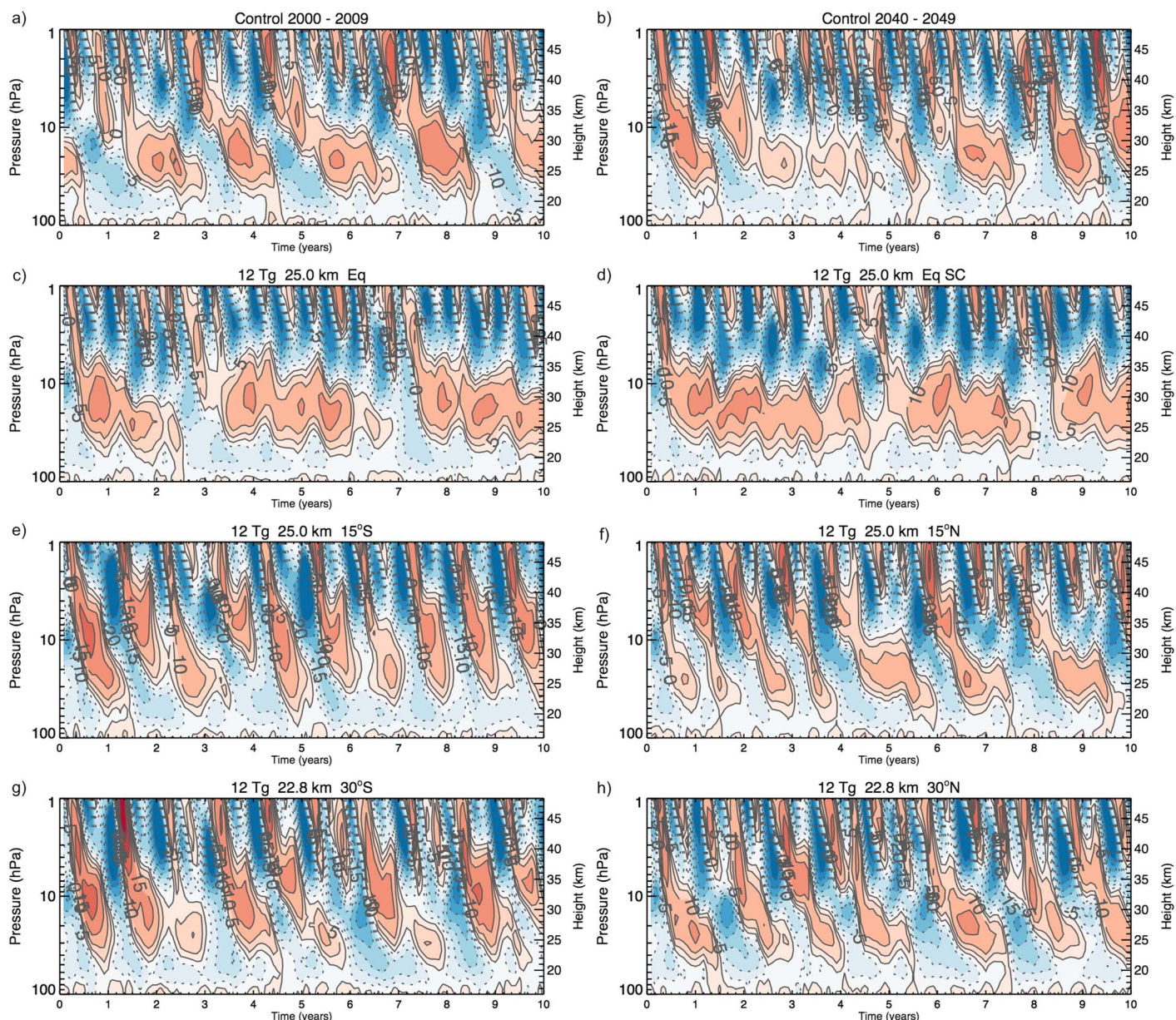
Figure 8. Zonal mean zonal wind averaged between 2°S and 2°N. (a) Results for the control simulation between 2000 and 2009, (b) results for the control simulation averaged between 2040 and 2049. Subsequent panels show zonal mean wind between 2040 and 2049 for the six simulations with SO$_2$ injections: (c) Equatorial, (d) Equatorial with SC, (e) 15°S, (f) 15°N, (g) 30°S, and (h) 30°N.

Figures 8a and 8b show the QBO for the control simulation for years 2000–2009 and 2040–2049, respectively. The mean QBO period in the control simulation is ∼24 months (Mills et al., 2017). Changes in climate between the earlier and later decades reveal a slightly altered QBO, with the westerly phase lengthening in a couple of the cycles, and the easterly phases becoming shorter. These changes are primarily due to increased parameterized gravity wave source momentum flux, which depends on changes in convection (Figure 9). Eastward gravity wave (GW) momentum flux near 100 hPa increases by 15% at the equator, and westward GW momentum flux increases by 20% at the equator. These changes in gravity wave fluxes will act to speed up the QBO. Changes in EP flux divergence and vertical advection are rather small (Figure 10), and comparisons of the black dashed and black solid lines in the panels show that the primary differences between the QBO in the control simulations between 2040–2049 and 2000–2009 come from differences in gravity wave drag. Figures 8c and 8d show that in the presence of 12 Tg SO$_2$ yr^{-1} equatorial injection, the QBO period lengthens to ∼42 months in the CESM1 (WACCM) simulation with fully interactive chemistry; however, it remains in a persistent westerly
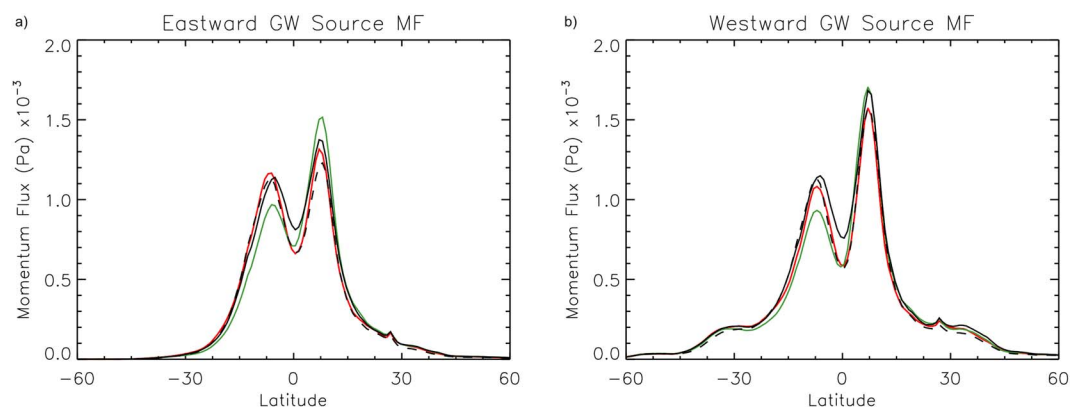
Figure 9. (a) Eastward and (b) westward gravity wave momentum flux at 100 hPa as a function of latitude averaged over 10 years of simulations: control 2000–2009 (black dashed), control 2040–2049 (black solid), 12 Tg SO_2 yr^{-1} Equatorial 2040–2049 (red), and 12 Tg SO_2 yr^{-1} 15°S 2040–2049 (green).

phase in the CESM1(WACCM) SC simulation. The near disappearance of the QBO via a prolonged westerly QBO phase seen in Figure 8b is consistent with previous studies of the response of QBO to SO_2 injections (Aquila et al., 2014); however, it is surprising that the same is not true in the IC simulation. The 10 year averages of equatorial zonal mean winds for these simulations are compared to the control in Figure 10a, showing stronger westerlies below 10 hPa, and stronger easterlies above 10 hPa. In the IC and SC simulations with equatorial 12 Tg SO_2 injections, the residual vertical velocity, and hence vertical advection, increases near the equator (as shown in Figure 4), which changes the balance of forcing terms driving the QBO. Figures 10b–10d show that the largest changes in the QBO between the simulations with SO_2 injections and the reference simulation come primarily from changes in the vertical advection and gravity wave drag. Vertical advection in the simulations with 12 Tg SO_2 yr^{-1} between 20 and 40 hPa is much greater as compared to the reference simulation (Figure 10b), opposing the GW drag and hence impeding the downward propagation of the QBO phases. EP flux divergence from resolved waves and meridional advection are very similar between the simulations. Vertical advection between 5 and 15 hPa is also much larger than in the control simulation.

GW drag also increases in magnitude in the simulations with SO_2 injections as compared to control. As shown in Figure 9, tropospheric cooling results in a decrease in the momentum flux of gravity waves at 100 hPa, driving changes in the mean flow that oppose the changes in vertical advection. GW drag is very responsive to the mean flow: stronger westerlies below 20 hPa caused by changed vertical advection will cause more eastward gravity waves to break in that region, and stronger easterlies above 20 hPa will cause more westward propagating gravity waves to break. Figure 10b also shows that the vertical advection term differs between the IC and SC simulations with 12 Tg yr^{-1} SO_2 injection, primarily above 10 hPa, but also between 20 and 40 hPa. As shown in Figures 4a and 4b, the residual vertical velocity increases more above 10 hPa in the SC simulation as compared to the IC simulation, as a result of differences in ozone heating. In short, interactive chemistry changes the heating and momentum budgets in the tropical stratosphere, causing notable changes to the QBO. A simulation with CESM1(WACCM) involving 24 Tg SO_2 yr^{-1} injection (not shown) resulted in a QBO period that remained at ~3.5–4 years and never completely disappeared likely due to the interaction with ozone. This demonstrates that the inclusion of interactive chemistry is important to the heat and momentum budget of the stratosphere, and the lack of its inclusion may lead to erroneous conclusions about changes in tropical dynamics, including the QBO. Our result is similar to Aquila et al. (2014) with respect to the prolongation of the QBO westerly phase following a stratospheric sulfate injection. However, Aquila et al. (2014) find that a 5 Tg yr^{-1} sulfate injection locks the QBO phase despite the inclusion of interactive chemistry. The difference might be due to the chemical processes included (for instance Aquila et al., 2014, did not include changes in photolysis rates due to the presence of aerosol) or to the differences in parameterizations of gravity waves driving the QBO.

Figures 8e–8h show the QBO for simulations involving injections of 12 Tg SO_2 yr^{-1} at 15°S, 15°N, 30°S, and 30°N, respectively. These panels show that unlike equatorial injections, SO_2 injections poleward of the equator, even at 15°S and 15°N, act to speed up the QBO instead of slowing it down. The QBO period is ~12 months in the simulations with injections at 15°S and ~17 months in the simulations with injections at 15°N, 30°S,
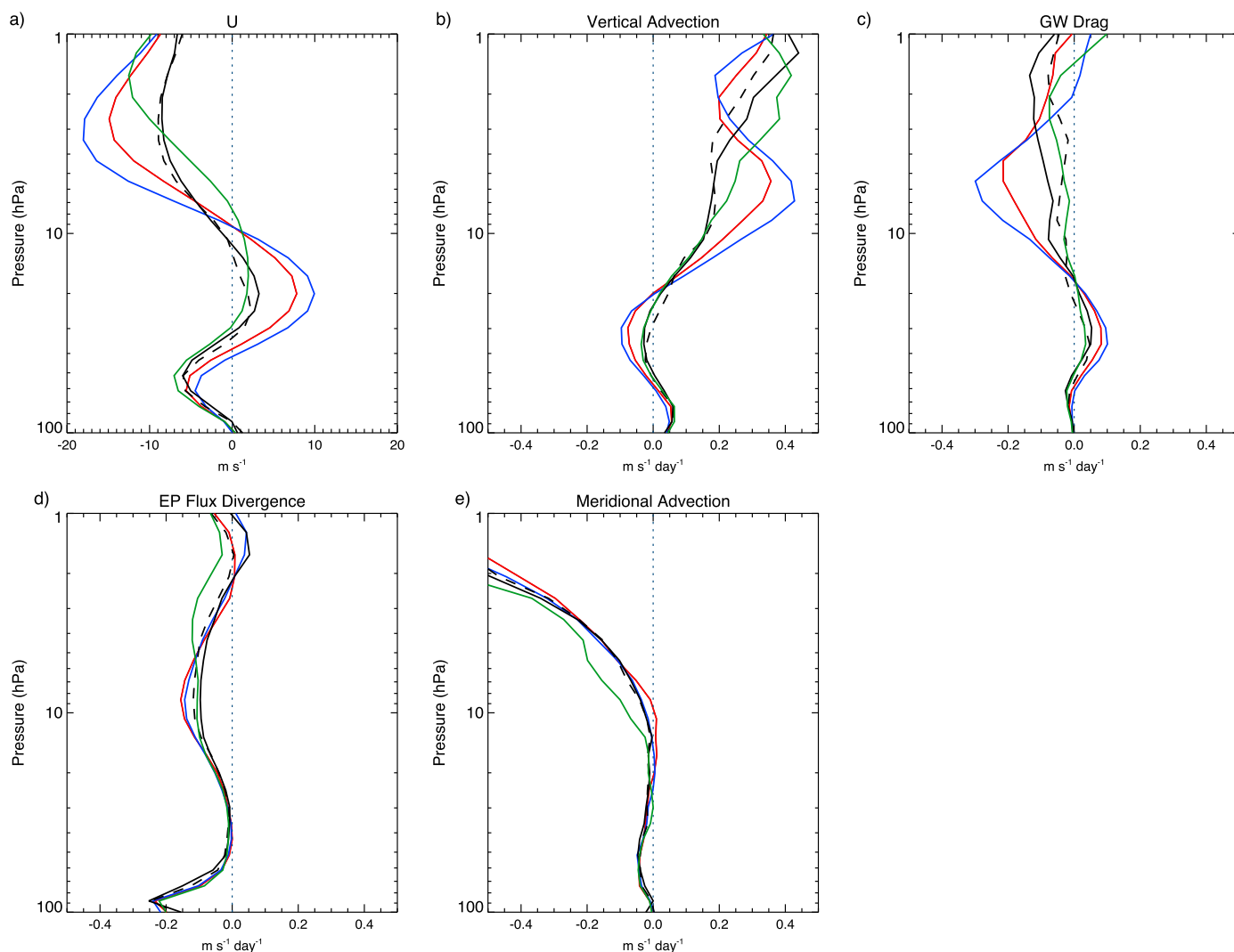
Figure 10. Zonal and latitudinal (2°S–2°N) average of (a) Zonal mean wind, (b) vertical advection, (c) gravity wave drag, (d) EP Flux divergence, and (e) meridional advection, averaged over 10 years of simulations: control 2000–2009 (black dashed), control 2040–2049 (black solid), 12 Tg Equatorial 2040–2049 (red), 12 Tg SO_2 yr^{-1} equatorial SC 2040–2049 (blue), and 12 Tg SO_2 yr^{-1} 15°S 2040–2049 (green). Zonal mean wind is in m s^{-1}; the rest of the quantities are in m s^{-1} d^{-1}.

and 30°N. These changes to the QBO can again be explained by examining the QBO forcing terms, especially the vertical advection term. Figures 4d–4f show that the residual vertical velocity changes primarily poleward of the equator in the simulations with SO_2 injections at 15°S, 15°N, 30°S, and 30°N, and the changes are small right at the equator. Hence, the vertical advection term is similar or smaller in magnitude to that of the control simulation, meaning the QBO is not expected to disappear. The main QBO forcing terms are shown in Figure 10 for the simulation with 15°S injection. Vertical advection, gravity wave drag, and EP flux divergence are fairly similar to those of the control simulations. The largest change is found in the meridional and vertical advection terms above 15 hPa (Figures 10b and 10e). The oscillation in the tropical zonal mean wind not only has a faster period but is also at higher altitudes as compared to the control and the simulations with equatorial SO_2 injections. These differences are likely are a result of the changed meridional advection term above 15 hPa; however, it is not obvious from the 10 year averaged momentum budget why the QBO period decreases to 12 months in the simulation with 15°S injection. Wave mean flow interactions in the QBO are complex, and the interactions and intricacies of the mechanisms that drive the QBO cannot be understood by evaluating average momentum budgets. In the 10 year mean, the zonal mean wind in the simulation with 15°S injection is very similar to control (Figure 10a), and the individual momentum budget terms reflect that.

4. Summary and Conclusions

We have performed a detailed analysis of changes in the stratospheric dynamical response, including the QBO, to SO_2 injections at various latitudes using a fully coupled Earth system model, CESM1(WACCM). We considered the response to 12 Tg SO_2 yr^{-1} injections 5 km above the tropopause at the equator, 15°S, 15°N, 30°S, and 30°N. Most of the simulations here were carried out with a fully interactive chemistry version of CESM1(WACCM). To isolate the role of interactive ozone on stratospheric dynamics, an additional simulation with specified chemistry was performed. We found that in all of the simulations, the lower tropical stratosphere warms as a result of SO_2 injections. The largest heating (~7 K) is associated with equatorial injections. In simulations with injections farther away from the equator, stratospheric heating still primarily occurred between 30°S and 30°N, despite the fact that the aerosols were primarily contained to the hemisphere of injection. The warming of the tropical lower stratosphere in our simulations was caused by a combination of longwave and shortwave heating in the aerosol layer, dynamical heating, and shortwave and longwave heating changes due to changes in atmospheric chemistry, primarily ozone. Stratospheric ozone increases by 1.2 ppm (~12 %) above and decreases by 0.8 ppm (~14%) in the SO_4 aerosol layer in the equatorial injection simulation, significantly altering the SW heating rates in those regions. As a result, changes in the residual vertical velocity and hence the Brewer Dobson circulation differ between the IC and SC simulations. This suggests that studies using models without interactive chemistry will not capture all of the stratospheric heating changes.

In this work, we also examined changes to the QBO as a result of SO_2 injections at various latitudes. In the CESM1(WACCM) simulation with equatorial 12 Tg SO_2 yr^{-1} injection, the QBO period increased to ~3.5 years, whereas when ozone is specified and unchanging, the oscillation almost completely disappears, and lower stratospheric equatorial winds become primarily westerly. Aquila et al. (2014) also found that the QBO completely disappeared in a simulation with an equatorial 5 Tg yr^{-1} SO_2 injection using the Goddard Earth Observing System Chemistry Climate model. The simulations shown here were performed with a fully coupled Earth system model including an interactive ocean and a gravity wave parameterization that responds to changes in convection. Although our approach accounts for most of the major processes and feedbacks between tropospheric and stratospheric processes, our results point to the need of thoroughly understanding and validating the components of the physical system that alter stratospheric dynamics: aerosol heating, dynamics, chemistry, and gravity wave parameterizations. Validation of aerosol properties and radiative forcing over recent decades of volcanic eruption (Mills et al., 2016, 2017) provide confidence in the ability of CESM1(WACCM) to calculate most relevant processes. CESM1(WACCM) is to our knowledge the best-validated global model of stratospheric aerosol properties. The most significant uncertainties remaining relate to subgridscale evolution of aerosol resulting from dense SO_2 plumes that would be emitted under geoengineering, as well as the validation of aerosol properties calculated under constant emission scenarios to the extent that they result in particles of larger size than those from volcanic eruptions. Cloud aerosol interactions in the troposphere are not as well understood and are a source of uncertainties in all Earth system models. As per atmospheric dynamics, the QBO in particular is very sensitive to changes in parameterized gravity wave drag, which is in turn dependent on changes in the convective heating calculated from the convection parameterization. An assessment of validity of both the convective and gravity wave parameterizations in future climate is needed to gain confidence in the possible changes to the QBO presented here. Resolved wave forcing and the QBO itself are also dependent on the vertical resolution of the model which is relatively coarse here. Higher vertical resolution allows for more upward propagation of Kelvin and Rossby gravity waves, and this changes the balance of momentum driving the QBO between the parameterized and resolved waves. Under a warming scenario, and in the presence of SO_2 injections, changes to resolved wave forcing of the QBO may be different compared to those in the current model in which majority of the QBO forcing comes from parameterized gravity waves. We plan to repeat some of the experiments presented here with a higher vertical resolution version of CESM1(WACCM) to gain confidence in our findings. In addition, because of the uncertainties inherent to the complex Earth system model used here, it is important to validate results of this study in a different modeling framework.

References

Andrews, D. G., Holton, J. R., & Leovy, C. B. (1987). *Middle atmosphere dynamics*. San Diego, CA: Academic Press.

Aquila, V., Garfinkel, C. I., Newman, P. A., Oman, L. D., & Waugh, D. W. (2014). Modifications of the quasi-biennial oscillation by a geoengineering perturbation of the stratospheric aerosol layer. *Geophysical Research Letters*, *41*, 1738–1744. https://doi.org/10.1002/2013GL058818

Bluth, G. J., Doiron, S. D., Schnetzeler, C. C., Krueger, A. J., & W. L. S. (1992). Global tracking of the SO_2 clouds from the June, 1991 Mount Pinatubo eruption. *Geophysical Research Letters*, *19*(2), 151–154.

Butchart, N. (2014). The Brewer-Dobson circulation. *Review of Geophysics*, *52*, 157–184. https://doi.org/10.1002/2013RG000448

Computational and Information Systems Laboratory (2012). *Yellowstone: IBM iDataPlex System (NCAR Strategic Capability Projects)*. Boulder, CO: UCAR/NCAR. https://doi.org/http://n2t.net/ark:/85065/d7wd3xhc

Crutzen, P. J. (2006). Albedo enhancement by stratospheric sulfur injections: A contribution to resolve a policy dilemma? *Climatic Change*, *77*(3–4), 211–219. https://doi.org/10.1007/s10584-006-9101-y

Danabasoglu, G., Bates, S. C., Briegleb, B., Jayne, S. R., Jochum, M., Large, W. G., . . . Yeager, S. G. (2012). The CCSM4 ocean component. *Jounral of Climate*, *25*, 1361–1389. https://doi.org/10.1175/JCLI-D-11-00091.1

Driscoll, S., Bozzo, A., Gray, L. J., Robock, A., & Stenchikov, G. (2012). Coupled Model Intercomparison Project 5 (CMIP5) simulations of climate following volcanic eruptions. *Journal of Geophysical Research*, *117*, D17105. https://doi.org/10.1029/2012JD017607

English, J. M., Toon, O. B., & Mills, M. J. (2012). Microphysical simulations of sulfur burdens from stratospheric sulfur geoengineering. *Atmospheric Chemistry and Physics*, *12*, 4775–4793. https://doi.org/10.5194/acp-12-4775-2012

Ferraro, A. J., Highwood, E. J., & Charlton-Perez, A. J. (2011). Stratospheric heating by potential geoengineering aerosols. *Geophysical Research Letters*, *38*, L24706. https://doi.org/10.1029/2011GL049761

Ferraro, A. J., Highwood, E. J., & Charlton-Perez, A. J. (2014). Weakened tropical circulation and reduced precipitation in response to geoengineering. *Environmental Research Letters*, *1*, 014001. https://doi.org/10.1088/1748-9326/9/1/014001

Ferraro, A. J., Charlton-Perez, A. J., & Highwood, E. J. (2015). Stratospheric dynamics and midlatitude jets under geoengineering with space mirrors and sulfate and titania aerosols. *Journal of Geophysical Research: Atmospheres*, *120*, 414–429. https://doi.org/10.1002/2014JD022734

Guenther, A. B., Jiang, X., Heald, C. L., Sakulyanontvittaya, T., Duhl, T., Emmons, L. K., & Wang, X. (2012). Model development the Model of Emissions of Gases and Aerosols from Nature version 2. 1 (MEGAN2. 1): An extended and updated framework for modeling biogenic emissions. *Geoscientific Model Development*, *5*, 1471–1492. https://doi.org/10.5194/gmd-5-1471-2012

Heckendorn, P., Weisenstein, D., Fueglistaler, S., Luo, B. P., Rozanov, E., Schraner, M., . . . Peter, T. (2009). The impact of geoengineering aerosols on stratospheric temperature and ozone. *Environmental Research Letters*, *4*, 045108. https://doi.org/10.1088/1748-9326/4/4/045108

Holland, M. M., Bailey, D. A., Briegleb, B. P., Bonnie, L., & Hunke, E. (2012). Improved sea ice shortwave radiation physics in CCSM4: The impact of melt ponds and aerosols on Arctic sea ice. *Journal of Climate*, *25*, 1413–1430. https://doi.org/10.1175/JCLI-D-11-00078.1

Jones, A. C., Haywood, J. M., & Jones, A. (2016). Climatic impacts of stratospheric geoengineering with sulfate, black carbon and titania injection. *Atmospheric Chemistry and Physics*, *16*(5), 2843–2862. https://doi.org/10.5194/acp-16-2843-2016

Kinnison, D. E., Brasseur, G. P., Walters, S., Garcia, R. R., Marsh, D. R., Sassi, F., . . . Simmons, A. J. (2007). Sensitivity of chemical tracers to meteorological parameters in the MOZART-3 chemical transport model. *Journal of Geophysical Research*, *112*, D20302. https://doi.org/10.1029/2006JD007879

Kravitz, B., Macmartin, D. G., Mills, M. J., Tilmes, S., Richter, J. H., Lamarque, J.-F., . . . Vitt, F. (2017). First simulations of designing stratospheric sulfate aerosol geoengineering to meet multiple simultaneous climate objectives. *Journal of Geophysical Research: Atmospheres*, *122*. https://doi.org/10.1002/2017JD026874

Lawrence, D., Oleson, K., Flanner, M., Thornton, P., Swenson, S., Lawrence, P., . . . Slater, A. (2011). Parameterization improvements and functional and structural advances in Version 4 of the Community Land Model. *Journal of Advances in Modeling Earth Systems*, *3*(3), M03001. https://doi.org/10.1029/2011MS000045

Liu, X., Easter, R. C., Ghan, S. J., Zaveri, R. A., & Rasch, P. J. (2012). Toward a minimal. representation of aerosols in climate models: Description and evaluation in the Community Atmosphere Model CAM5. *Geoscientific Model Development*, *5*, 709–739.

MacMartin, D. G., Kravitz, B., Tilmes, S., Richter, J. H., Michael, M. J., Lamarque, J.-F., & Tribbia, J. J. (2017). The climate response to stratospheric aerosol geoengineering can be tailored using multiple injection locations. *Journal of Geophysical Research: Atmospheres*, *122*. https://doi.org/10.1002/2017JD026868

Mills, M. J., Richter, J. H., Tilmes, S., Macmartin, D. G., Kravitz, B., Tribbia, J. J., & Vitt, F. (2017). Radiative and chemical response to interactive stratospheric aerosols in fully coupled CESM1 (WACCM). *Journal of Geophysical Research: Atmospheres*, *122*. https://doi.org/10.1002/2017JD027006

Mills, M. J., Schmidt, A., Easter, R., Solomon, S., Kinnison, D. E., Ghan, S. J., . . . Gettelman, A. (2016). Global volcanic aerosol properties derived from emissions, 1990–2014, using CESM1(WACCM). *Journal of Geophysical Research: Atmospheres*, *121*, 2332–2348. https://doi.org/10.1002/2015JD024290

Morgenstern, O., Hegglin, M., Rozanov, E., O'Connor, F., Luke Abraham, N., Akiyoshi, H., . . . Zeng, G. (2017). Review of the global models used within phase 1 of the Chemistry-Climate Model Initiative (CCMI). *Geoscientific Model Development*, *10*(2), 639–671. https://doi.org/10.5194/gmd-10-639-2017

Neale, R. B., Chen, C.-C., Gettelman, A., Lauritzen, P. H., Park, S., Williamson, D. L., . . . Rasch, P. J. (2012). Description of the NCAR Community Atmosphere Model (CAM 5.0) (NCAR Technical Note). Boulder, Colo: NCAR TN(486).

Niemeier, U., Schmidt, H., & Timmreck, C. (2011). The dependency of geoengineered sulfate aerosol on the emission strategy. *Atmospheric Science Letters*, *12*(2), 189–194. https://doi.org/10.1002/asl.304

Niemeier, U., & Timmreck, C. (2015). What is the limit of climate engineering by stratospheric injection of SO_2? *Atmospheric Chemistry and Physics*, *15*(16), 9129–9141. https://doi.org/10.5194/acp-15-9129-2015

NRC (2015). *Climate intervention: Reflecting sunlight to cool Earth*. Washington, DC: The National Academies Press. https://doi.org/10.17226/18988

Pitari, G., Aquila, V., Kravitz, B., Robock, A., Watanabe, S., Cionni, I., . . . Tilmes, S. (2014). Stratospheric ozone response to sulfate geoengineering: Results from the Geoengineering Model Intercomparison Project (GeoMIP). *Journal of Geophysical Research: Atmospheres*, *119*, 2629–2653. https://doi.org/10.1002/2013JD020566

Portmann, R. W., Solomon, S., Garcia, R. R., Thomason, L. W., Poole, L. R., & Mccormick, M. P. (1996). Role of aerosol variations in anthropogenic ozone depletion in the polar regions paper C1ONO. *Journal of Geophysical Research*, *101*, 22,991–23,006.

Rasch, P. J., Crutzen, P. J., & Coleman, D. B. (2008). Exploring the geoengineering of climate using stratospheric sulfate aerosols: The role of particle size. *Geophysical Research Letters*, *35*, L02809. https://doi.org/10. 1029/2007GL032179

Rasch, P. J., Tilmes, S., Turco, R. P., Robock, A., Oman, L., Chen, C.-C. J., . . . Garcia, R. R. (2008). An overview of geoengineering of climate using stratospheric sulphate aerosols. *Philosophical Transactions of the Royal Society of London A: Mathematical, Physical and Engineering Sciences*, *366*(1882), 4007–4037. https://doi.org/10.1098/rsta.2008.0131

Richter, J. H., Sassi, F., & Garcia, R. R. (2010). Towards a physically based gravity wave source parameterization in a general circulation model. *Journal of Atmospheric Sciences*, *67*, 136–156.

Robock, A., Oman, L., & Stenchikov, G. L. (2008). Regional climate responses to geoengineering with tropical and Arctic SO_2 injections. *Journal of Geophysical Research*, *113*(16), 1–15. https://doi.org/10.1029/2008JD010050

Smith, K. L., Neely, R. R., Marsh, D. R., & Polvani, L. M. (2014). The Specified Chemistry Whole Atmosphere Community Climate Model (SC-WACCM). *Journal of Advances in Modeling Earth Systems*, *6*(3), 883–901. https://doi.org/10.1002/2014MS000346

Solomon, S., Portmann, R. W., Garcia, R. R., Thomason, L. W., Poole, L. R., & McCormick, M. P. (1996). The role of aerosol variations in anthropogenic ozone depletion at northern midlatitudes. *Journal of Geophysical Research*, *101*(D3), 6713–6727. https://doi.org/10.1029/95JD03353

Stenchikov, G., Robock, A., Ramaswamy, V., Schwarzkopf, M. D., Hamilton, K., & Ramachandran, S. (2002). Arctic Oscillation response to the 1991 Mount Pinatubo eruption: Effects of volcanic aerosols and ozone depletion. *Journal of Geophysical Research*, *107*(24), 4803. https://doi.org/10.1029/2002JD002090

Tie, X., & Brasscur, G. (1995). The response of stratospheric ozone to volcanic eruptions: Sensitivity to atmospheric chlorine loading. *Geophysical Research Letters*, *22*(22), 3035–3038.

Tilmes, S., Garcia, R. R., Kinnison, D. E., Gettelman, A., & Rasch, P. J. (2009). Impact of geoengineered aerosols on the troposphere and stratosphere. *Journal of Geophysical Research*, *114*, D12305. https://doi.org/10.1029/2008JD011420

Tilmes, S., Kinnison, D. E., Garcia, R. R., Salawitch, R., Canty, T., Lee-Taylor, J., . . . Chance, K. (2012). Impact of very short-lived halogens on stratospheric ozone abundance and UV radiation in a geo-engineered atmosphere. *Atmospheric Chemistry and Physics*, *22*(12), 10,945–10,955. https://doi.org/10.5194/acp-12-10945-2012

Tilmes, S., Muller, R., & Ross, S. (2008). The sensitivity of polar ozone depletion to proposed geoengineering schemes simone tilmes. *Science*, *320*(1201). https://doi.org/10.1126/science.1153966

Tilmes, S., Richter, J. H., Mills, M. J., Kravitz, B., MacMartin, D., & Vitt, F. (2017). Sensitivity of stratospheric SO_2 injection locations on aerosol distribution and climate response. *Journal of Geophysical Research: Atmospheres*, *122*. https://doi.org/10.1002/2017JD026888